Article

A Self-Consistent Return Stroke Model That Includes the Effect of the Ground Conductivity at the Strike Point

Vernon Cooray [1],*, Marcos Rubinstein [2] and Farhad Rachidi [3]

1 Department of Electrical Engineering, Uppsala University, 752 37 Uppsala, Sweden
2 HEIG-VD—Haute Ecole d'Ingénierie et de Gestion du Canton de Vaud, University of Applied Sciences and Arts Western Switzerland, 1401 Yverdon-les-Bains, Switzerland; marcos.rubinstein@heig-vd.ch
3 Electromagnetic Compatibility Laboratory, Swiss Federal Institute of Technology (EPFL), 1015 Lausanne, Switzerland; farhad.rachidi@epfl.ch
* Correspondence: vernon.cooray@angstrom.uu.se

Abstract: A current generation type return stroke model which can take into account the possible modifications of the return stroke properties by the soil conductivity at the strike point of the lightning flash is introduced. The model is also capable of incorporating the reflection of the current at the ground end of the return stroke channel. In this paper, this return stroke model is used to investigate (a) the effect of the ground conductivity at the strike point on the source electromagnetic fields generated by return strokes and (b) the effect of current reflection at ground level on the electromagnetic field generated by return strokes. The source electromagnetic fields are the electromagnetic fields generated by lightning flashes calculated in such a way that they are not distorted by propagation effects. The results obtained show that the ground conductivity at the strike point does not significantly influence the return stroke current peak or the radiation field peak for ground conductivities higher than about 0.001 S/m. However, strike points with very poor conductivities (lower than 0.001 S/m) would result in a decrease of the peak electric field. In contrast to the peak values of the lightning current and the electric field, the peak values of the time derivatives of the lightning current and electric field are significantly reduced when the strike point of the lightning flash is located over a finitely conducting ground. The inclusion of the current reflection at ground level influences significantly the saturation of the close electric fields. The current reflection also gives rise to residual electric fields, a difference in the field levels generated by the dart leader and the return stroke. The residual field decreases as the fraction of the reflected current decreases.

Keywords: lightning; return stroke; stepped leader; dart leader; return stroke models; current reflection; ground conductivity

1. Introduction

Return stroke models can be divided into the following categories depending on the basic principles used in constructing them: physical models, transmission line models, antenna models, electromagnetic models, and engineering models [1]. Engineering models are the simplest, yet they are highly successful in predicting electromagnetic fields of return strokes at different distances from the lightning channel. The engineering models available in the literature can be divided into three types, namely, Current Propagation (CP), Current Generation (CG), and Current Dissipation (CD) [1]. One of the simplest CP type models where the return stroke current propagates without attenuation and dispersion was introduced by Uman and McLain [2]. Both Nucci et al. [3] and Rakov and Dulzon [4] introduced current attenuation into the CP type return stroke models. Cooray and Orville [5] and Cooray et al. [6] introduced CP type models that incorporate both current attenuation and current dispersion. Return stroke models that belonging to CG types were introduced by Heidler [7] and Diendorfer and Uman [8], among others. The concept of CD type return stroke models was first introduced by Cooray [9]. Return

stroke models that utilized both CG and CD concepts were introduced by Cooray and Diendorfer [10] and Cooray and Rakov [11].

Researchers use lightning return stroke models, mainly, to calculate the electromagnetic fields from lightning at different distances needed for engineering studies and, less frequently, to remote sense the source characteristics such as the return stroke current. Almost all of the engineering return stroke models use the channel-base current as an input; for this reason, they cannot be used to investigate the way in which external physical parameters such as the ground conductivity at the strike point affect the source characteristics, namely, the channel-base current and the electromagnetic fields.

In a recent study, Asfur et al. [12] discussed the effect of the conductivity of sea water on the return stroke current parameters by extrapolating the results obtained from experiments conducted using small sparks in the laboratory. They concluded that the salt content of the sea water and, hence, its conductivity can affect the return stroke current. On the other hand, theoretical results presented by Cooray and Rakov [11] (from here on referred to as CR) predict how the channel-base current is influenced by the ground conductivity. The study showed that conductivities larger than about 0.001 S/m do not influence the peak current of the return stroke. However, the current derivative can be seriously affected by the ground conductivity at the strike point.

In this paper, we will further develop the ideas introduced by CR to create a full-fledged subsequent return stroke model. A model based on the ideas introduced by CR to represent the first return strokes is under consideration (see Section 5). The return stroke model to be introduced here is capable of accommodating current reflection at ground level and it can predict the effect of the ground conductivity at the strike point on the return stroke current and on the source electromagnetic fields generated by return strokes. The source electromagnetic fields are the electromagnetic fields generated by the return stroke before they are distorted by the propagation effects along the path from the strike point to the measuring site. In this study, we will investigate the effect of current reflection and the effect of the ground conductivity at the strike point on the source electromagnetic fields. The current study is partly motivated by an experimental study conducted by Heidler and Hopf [13] where they claimed that the source electromagnetic fields generated by lightning striking a poorly conducting ground cannot be as fast as the ones generated by lightning flashes taking place under maritime conditions in Florida, USA. We will utilize the model to check the validity of the claim made by Hopf and Heidler [13].

2. Basic Concepts of the Model

In constructing the return stroke model, we will utilize the procedures developed previously by CR to investigate the effect of the ground conductivity on the return stroke current and how to include the current reflection at ground level. The procedure developed by CR is based on modelling the return stroke channel by combining the concepts of Current Generation (CG) and Current Dissipation (CD). Here, we will utilize the same procedure but with a few modifications.

In a CG type return stroke model, the input parameters could be any three of the following parameters: the channel-base current, the discharge time constant of the corona sheath, the charge deposited by the return stroke on the leader channel, and the return stroke speed. In many of the return stroke models, the channel-base current is selected as one of the input parameters [2–9]. However, as pointed out by CR, in order to investigate the effect of the ground conductivity on the return stroke current, the channel-base current has to be a model-predicted parameter rather than an input. For this reason, they selected the corona discharge time constant, the charge deposited by the return stroke on the leader channel, and the return stroke speed as input parameters. The model that is being used here to estimate the effect of the ground conductivity on the electromagnetic fields here is similar to that used by CR but with a few modifications. Here, we will develop a single model to incorporate both the effect of the ground conductivity and the current reflection at ground level. Let us now provide the details of the model.

2.1. Charge Deposited by the Return Stroke

In a study conducted by Cooray et al. [14], the return stroke current waveforms of downward negative lightning flashes measured by Berger [15] were utilized to obtain the charge brought to ground during the first 100 µs of the first return stroke and the first 50 µs of the subsequent return strokes. They found a strong correlation between the return stroke peak current and the charge transferred to ground by return strokes. Combining this information with the bi-directional leader concept [16], they investigated how this charge was distributed along the stepped and dart leader channels. The results of that study show that the charge per unit length along a fully extended down-coming leader channel can be approximated by

$$\rho_l(z) = a_0\left(1 - \frac{z}{H}\right)I_p + \frac{(a+bz)}{1 + cz + dz^2}I_p \tag{1}$$

In the above equation, z is the vertical height of the point of interest (in meters), H is the total length (in meters) of the leader channel which is assumed to be vertical, $\rho_l(z)$ (in C/m) is the charge per unit length of the leader channel at height z and I_p is the peak return stroke current in kA. a_o, a, b, c, and d are constant parameters which are given by:

- for stepped leaders (preceding first return strokes), $a_0 = 1.476 \times 10^{-5}$, $a = 4.857 \times 10^{-5}$, $b = 3.909 \times 10^{-6}$, $c = 0.522$, $d = 3.73 \times 10^{-3}$;
- for dart leaders (preceding subsequent return strokes), $a_0 = 5.09 \times 10^{-6}$, $a = 1.325 \times 10^{-5}$, $b = 7.06 \times 10^{-6}$, $c = 2.089$, $d = 1.492 \times 10^{-2}$.

Observe that Equation (1) represents the charge distribution of a fully extended (i.e., one end at ground level) leader channel of length H corresponding to a return stroke peak current of I_p.

Cooray [17] utilized the expression for the leader charge distribution given by Equation (1) to estimate the distribution of charge per unit length deposited by the return stroke on the leader channel. In deriving this, he appealed again to the same bidirectional leader model that was utilized by Cooray et al. [14] in estimating the leader charge distribution given by Equation (1). According to the bidirectional leader model, during the return stroke process, in addition to neutralizing the negative charge already located on the leader channel (we are considering a negative return stroke here), additional positive charge will be added along the channel. According to this work, the derived charge per unit length $\rho_{ret}(z)$ deposited by a return stroke as a function of the length along the channel z is given by

$$\rho_{ret}(z) = a_0 I_p + \frac{(a+bz)}{1 + cz + dz^2}I_p \tag{2}$$

In the above equation, I_p is the peak return stroke current in kA. Observe that Equation (2) represents the charge deposited by both first and subsequent return stroke currents. The parameters a_0, a, b, c, and d are the same as in Equation (1). Observe that the values of the parameters differ depending on whether it is the first or subsequent return strokes which are under consideration. In this paper, we will consider the subsequent return strokes. It is also important to point out that the charge distributions given by Equations (1) and (2) are based on static calculations and they neglect the time-dependence of the dart leader current. In reality, at the time at which the dart leader tip reaches the ground, the dart leader current peak occurs at a few tens of meters above the ground. This is the case because the dart leader current risetime is about 1 µs and the speed of the dart leader close to ground is about 10^7 m/s [18]. In order to take this into account, we will modify the charge distribution slightly by assuming that the peak of the distribution is reached not at ground level as in Equation (1) but at some height. This is done simply by multiplying the charge distributions by a factor $k(1 - e^{-z/\lambda})$:

$$\rho_l(z) = k(1 - e^{-z/\lambda})\left\{a_0\left(1 - \frac{z}{H}\right)I_p + I_p\frac{(a+bz)}{1 + cz + dz^2}\right\} \tag{3}$$

$$\rho_{ret}(z) = k(1 - e^{-z/\lambda}) \left\{ a_0 I_p + \frac{I_p(a + bz)}{1 + cz + dz^2} \right\} \tag{4}$$

In our analysis, we will select λ = 10 m to take into account the charging time of the dart leader (i.e., the risetime of the dart leader current). The charge deposited by a 12-kA peak current subsequent return stroke as given by Equation (4) is shown in Figure 1. Note that the charge deposited by the return stroke increases initially, reaches a peak within a few tens of meters, and decreases rapidly to a constant value. The parameter k is needed in the equation to match the model generated return stroke current peak to the value of I_p that appears in Equations (3) and (4). The value of k may change depending on the type of corona discharge time constant selected in the model. For the corona discharge time constant profile used in this paper (see the next section), we need k = 1.4.
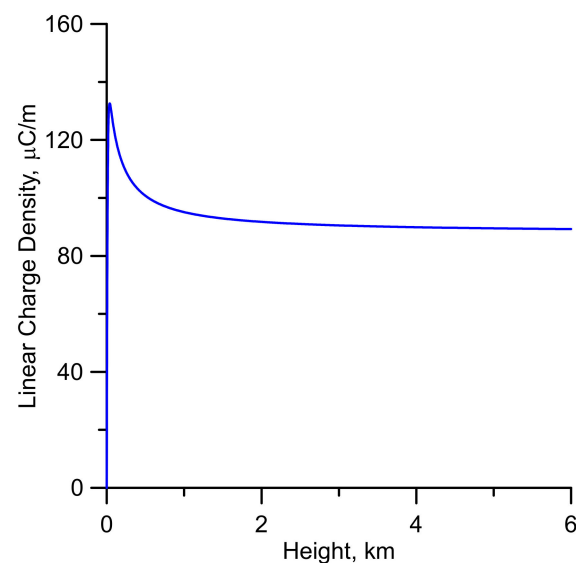

Figure 1. The charge deposited by a 12-kA subsequent return stroke as given by Equation (4).

2.2. Corona Discharge Time Constant

The corona discharge time constant defines how fast the charge that is being deposited on the leader channel is neutralized by the return stroke. The trigger for this neutralization process is the change of the potential of the central core of the leader channel from cloud potential to ground potential during the return stroke process. Two physical parameters control the rapidity at which the corona charge is neutralized. First, during the neutralization process, the central core's potential has to be changed from cloud potential to ground potential. This requires rapid heating followed by an increase in the conductivity of the core of the leader channel so that the ground potential is transferred into the leader channel. Second, the neutralization process is controlled by how fast the heating of the channel is achieved by transferring the energy in electrons to the ions and neutrals. This is called the thermalization. This transfer of energy from electrons to neutrals is completed in a matter of nanoseconds, which is the thermalization time [19]. The thermalization process sets the lowest time within which the corona sheath could be neutralized. On the other hand, how fast the leader channel potential in regions in the vicinity of the ground can be changed from cloud potential to ground potential depends on the electrical relaxation time constant of the ground. The relaxation time constant, τ_r, is given by $\varepsilon_0 \varepsilon_r / \sigma$ where σ is the ground conductivity and ε_r is the relative dielectric constant of the soil. The relaxation time increases with decreasing ground conductivity and so does the time necessary for the change of the channel potential from that of cloud to ground. In addition to these considerations, experimental data indicate that the risetime of the return stroke current increases with height [20]. Within the confines of the CG type models, an increase in the return stroke current risetime is caused by an increase in the corona discharge time constant

of the corona current. Taking all these points into consideration, the corona discharge time constant is defined as

$$\tau(z) = \tau_0 + \tau_s(1 - e^{-z^2/\lambda^2}) \tag{5}$$

$$\tau_0 = \tau_t \text{ if } \tau_r < \tau_t \tag{6}$$

$$\tau_0 = \tau_r \text{ if } \tau_r > \tau_t \tag{7}$$

In the above equations, τ_r is the relaxation time of the ground, τ_t is the thermalization time, τ_s and λ are constants, and z is the height along the channel. As can be seen from Equation (5), we assume that the corona discharge time constant increases initially with height, but it will reach a steady value at higher levels. The reason for this choice is based on the work conducted recently by Cooray et al. [6]. In that paper, the authors pointed out that in order to generate the frequently observed subsidiary peak in subsequent return stroke radiation fields and the hump in the close magnetic fields, the current risetime in the return stroke channel should increase initially, but should reach a more or less constant value after propagating several hundreds of meters along the channel. In the current model, the same results can be obtained by assuming the corona discharge time constant to vary in the above-mentioned manner. Based on the results presented by Cooray et al. [6] and after a preliminary evaluation of the effect of τ_s and λ on the radiation and close magnetic fields, we have selected $\tau_s = 10^{-6}$ s and $\lambda = 250$ m. As mentioned earlier, the thermalization time is in the order of nanoseconds. In the case of subsequent return strokes, we have selected the thermalization time to be 5 ns. This is close to the value selected by CR. Indeed, the thermalization time may depend on the volume of the discharge channel that is necessary to be thermalized and the background electric field to which the electrons are exposed during the thermalization process. If this electric field is larger and the volume of the discharge channel needed to be thermalized is smaller, then the thermalization time could be shorter than the value selected above. In this respect, the thermalization time could be much shorter in the case of small sparks where the background electric field is close to the electrical breakdown field in air throughout the whole volume and the volume needed to be thermalized is much smaller. Thus, in the case of small sparks, this time can be in the sub-nanosecond range. Indeed, this could be the case because the risetime of the currents in small sparks could be in the order of nanoseconds [21] indicating a thermalization time in the sub-nanosecond range. However, this is an important parameter in the model because it determines the lowest value of the relaxation time below which the current parameters would not be further changed. Further experiments with long sparks could help in pinpointing this value.

2.3. Return Stroke Speed

Observe from Figure 1 that the charge deposited by the return stroke remains approximately constant for heights above 1 km or so. Such a charge distribution in a CG type return stroke model will lead to a distant radiation field that remains above the zero line until the end of the return stroke is reached. The reason for this is the following. The peak value of the return stroke current at a given height depends on the amplitude of the corona current generated by the channel elements located in the vicinity of the return stroke front. If the deposited charge remains constant, the amplitude of the corona current also remains constant and this leads to a return stroke current that maintains its peak value with height. This will, in turn, generate a constant radiation field. Thus, in order to make the radiation field decay, it is necessary to terminate the channel. This can be done by restricting the return stroke channel length to about 5–6 km. However, such an artificial termination of the channel gives rise to a fast and large opposite overshoot in the radiation field that is not observed in the experiments (the so-called mirror-image effect). On the other hand, experimental data show that the return stroke channel does not terminate abruptly at cloud height but will turn towards horizontal and continue for many more kilometers [22]. A gradual turning of the return stroke channel from vertical to horizontal direction can lead to a slow decay of the radiation field similar to that observed experimentally [23]. Furthermore, experimental

observations also show that the return stroke speed decreases with height [24,25], and such a reduction in the speed of propagation of the return stroke will also produce a smooth zero crossing in the radiation field. Actually, both the above-mentioned effects could be influencing the decay of the return stroke radiation fields. However, in this paper, we will assume that the dominant role is played by the decrease in the return stroke speed. For this reason, the return stroke speed is assumed to decrease with height in the model according to the equation

$$v = v_0 e^{-z/\lambda_v} \tag{8}$$

where v_0 is 1.5×10^8 m/s and $\lambda_v = 2000$ m.

2.4. Current Reflection at Ground Level

CR provided theory that makes it possible to include current reflection in return stroke models that belong to the CG category. Even though they did not do it using the model described above, the technique they introduced can be used to include the current reflection in the present model. Consider the case where the total current at ground end generated by the downward moving corona current is completely reflected. In this scenario, we have to assume that only half of the total current at ground level is produced by the negative corona currents reaching the ground. This will be called the incident current, and it is modelled using the CG concept. That is, as the return stroke front travels along the leader channel, it will give rise to negative corona currents that travel down towards the ground creating the incident current component at ground level. We assume that it will be reflected completely at ground level; the reflected current carrying positive charge travels upwards with the speed of light. This current component will be described using the CD concept. In the CD concept, as the reflected current reaches a given channel element it will generate a negative corona current that travels upward with the speed of light. These upward moving corona currents carrying negative charge will dissipate the upward moving reflected current which is carrying positive charge upwards. As in the CG type models, in order to fully describe the variation of the upward moving reflected current using the CD concept, one has to define three input parameters out of the following four parameters: the reflected current at the channel base, the corona discharge time constant, the charge deposited along the channel by the reflected current, and the return stroke speed. In our case, the reflected current at the channel base, the return stroke speed and the corona discharge time constant are already defined. Note that the corona discharge time constant and the return stroke speed have to be the same for both the incident and reflected current. This is the case because the return stroke front speed and the physics of the discharge process are unique for a given return stroke (i.e., cannot be separated into components pertinent to incident and reflected current).

2.4.1. The Incident Current at Ground Level

The incident current at ground level is given by [1,26]

$$I_i(0,t) = \int_0^{h_e} i_{c,i}(\xi, t - \xi/v_{av}(\xi) - \xi/c)d\xi \, t > z/v_{av}(z) \tag{9}$$

In the above equation, $i_{c,i}(z,t)$ is the corona current at height z associated with the incident current and $v_{av}(z)$ is the average return stroke speed over the channel section from ground level to height z. The parameter h_e is the maximum length of the return stroke channel that contributes to the channel base current at time t. The corona current at height z and the average return stroke speed are given by

$$i_{c,i}(z) = \frac{\rho_{ret}(z)f}{\tau(z)} \exp\{-[t - z/v_{av}(z)]/\tau(z)\} t > z/v_{av}(z) \tag{10}$$

$$v_{av}(z) = z / \int_0^z \frac{dz}{v(z)} \tag{11}$$

According to our definition, f is the ratio of the amplitude of the incident current to the total current at the channel base. Note that f is different from the classical reflection coefficient which is defined as the ratio of the reflected current to the incident current. If $f = 1$, then no current is reflected and the total current at the channel base is the incident current. If $f = 0.5$, the incident current is completely reflected. One could introduce different amounts of current reflection by changing f from 1 to 0.5. Observe that in order to maintain the same total current at ground level, the magnitude of the incident current has to be changed when f changes from 1 to 0.5. For example, when $f = 1$ the peak amplitude of the incident current will be 12 kA and when $f = 0.5$ the peak of the incident current will be 6 kA.

2.4.2. The Reflected Current at Ground Level

According to our definition of f, if we represent the total current at the channel base as $I_b(t)$, the reflected current is given by

$$I_r(0, t) = (1 - f)I_b(t) \tag{12}$$

Recall that we will be modelling the reflected current component using the CD concept. In this scenario, the reflected current component travels upwards with the speed of light but it will be dissipated by the upward moving negative corona currents making the total current above the return stroke front, which is moving with speed $v(z)$, equal to zero. In order to complete the description of the reflected current at any height, we need the speed of propagation of the return stroke front, the discharge time constant, and the charge deposited by the reflected current along the leader channel. The speed of propagation of the return stroke front is given by Equation (8) and the discharge time constant was defined by Equations (5)–(7). What is needed is the charge per unit length deposited by the reflected current along the leader channel. This charge is different from the charge per unit length deposited on the leader channel by the incident current component. Observe that in our case the corona discharge time constant varies with height. Before we treat this case, let us consider the equations pertinent to the case where the corona discharge time constant does not vary with height. Let us represent the corona discharge time constant pertinent to this hypothetical case by τ_{con}. The charge per unit length deposited by the reflected current in this case is given by [9,27]

$$\rho_{ref}(z) = \left\{ \frac{v_{av}(z) - z\frac{dv_{av}(z)}{dz}}{\{v_{av}(z)\}^2} - \frac{1}{c} \right\} \left[I_r(0, z/v*) + \tau_{con} \frac{\partial I_r(0, z/v*)}{\partial t} \right] \tag{13}$$

$$v* = \frac{1}{v_{av}(z)} - \frac{1}{c} \tag{14}$$

Note that, in our case, the corona discharge time constant varies along the channel. However, observing that the corona current generated at a height z will start neutralizing the reflected current waveform from the time $z/v_{av}(z)$ and continue to neutralize the current for a time equal to the corona discharge time constant $\tau(z)$, the above equation will still be valid if the corona discharge time constant does not change significantly over the distance travelled by the return stroke from height z over the time $\tau(z)$. Thus, if

$$\tau(z)v(z)\frac{\partial \tau(z)}{\partial z} << \tau(z) \tag{15}$$

or

$$v(z)\frac{\partial \tau(z)}{\partial z} << 1 \tag{16}$$

the charge deposited by the reflected component of the current can be obtained by replacing τ_{con} in Equation (13) by $\tau(z)$. That is

$$\rho_{ref}(z) = \left\{ \frac{v_{av}(z) - z\frac{dv_{av}(z)}{dz}}{\{v_{av}(z)\}^2} - \frac{1}{c} \right\} \left[I_r(0, z/v*) + \tau(z)\frac{\partial I_r(0, z/v*)}{\partial t} \right] \qquad (17)$$

Since the condition given by Equation (16) is valid in our case, the charge deposited per unit length along the leader channel by the reflected current is given by Equation (17).

Now, all the parameters of the model necessary to investigate the effect of the ground conductivity at the strike point and the current reflection on the return stroke generated electromagnetic fields are defined. In the next section, we will describe the equations pertinent to the calculation of electromagnetic fields.

2.5. Calculation of Electromagnetic Fields

Once the return stroke speed and the current along the channel are specified, it is a simple matter to calculate the electromagnetic fields. The electromagnetic fields generated by the CG and CD type models can be expressed rather conveniently using the charge accelerating technique [28]. Let us first consider the fields produced during the generation of the incident current and subsequently the ones generated by the reflected current.

2.5.1. Electromagnetic Fields Generated by the Incident Current Component

In general, the charge acceleration technique describes the components of the electromagnetic field as Static or Coulomb fields produced by stationary charges, Velocity or modified Coulomb fields produced by moving charges, and Radiation fields produced by accelerating charges. In the CG type models, radiation fields are generated during the initiation of the corona currents and during their termination at ground level. In CG models, the corona currents propagate downwards with the speed of light and, therefore, the velocity fields associated with these currents is equal to zero [28]. As the return stroke front reaches a given channel section, negative corona current leaves that channel section leaving behind a positive charge. This positive charge will generate an electrostatic field. Thus, the total electromagnetic field can be described as a summation of radiation and static fields. Consider the processes taking place in a channel element dz located at height z when the return stroke front reaches that element. The geometry relevant for the calculation is shown in Figure 2. The arrival of the return stroke front at the channel element will generate a corona current which will travel down towards ground at the speed of light. At the same time, it will leave behind a stationary positive charge which is given by the time integral of the corona current. The radiation field generated at ground level by the initiation of the corona current is [28]

$$dE_{1,inc} = \frac{i_{c,i}(z, t - r/c)}{2\pi\varepsilon_0 cr} \frac{\sin^2\theta}{1 - \cos\theta} dz \qquad (18)$$

where the corona current is given by Equation (10). The total radiation field generated by the initiation of corona currents along the return stroke channel is given by

$$E_{1,inc}(t) = \int_0^L \frac{i_{c,i}(z, t - r/c)}{2\pi\varepsilon_0 cr} \frac{\sin^2\theta}{1 - \cos\theta} dz \qquad (19)$$

Note that L is the apparent height of the return stroke as measured by an observer at the point where the electromagnetic field is calculated. Thus, L is a parameter that varies with time. As the corona current reaches the ground, it will be absorbed, and this will give rise to a radiation field

$$E_{2,inc} = -\frac{I_i(0, t - D/c)}{2\pi\varepsilon_0 cD} \qquad (20)$$
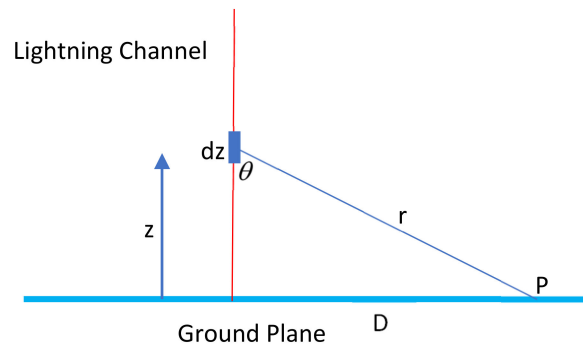
Figure 2. The geometry relevant to the calculation of the electromagnetic fields.

Consider again a channel element at height z. The positive charge as a function of time that will remain in the channel element as the negative charge leaves the element in the form of corona current is given by

$$q_i(z,t)dz = dz \int_{z/v_{av}(z)}^{t} i_{c,i}(z,t)dt \tag{21}$$

The static field produced by this charge at the point of observation is

$$dE_{3,inc}(t) = \frac{q_i(z, t - r/c)}{2\pi\varepsilon_0 r^2} \cos\theta dz \tag{22}$$

The total static field produced by the static charges accumulated along the channel is given by

$$E_{3,inc}(t) = \int_0^L \frac{q_i(z, t - r/c)}{2\pi\varepsilon_0 r^2} \cos\theta dz \tag{23}$$

Combining all the equations together, the total electric field produced during the generation of the incident current is given by

$$E_{inc}(t) = E_{1,inc}(t) + E_{2,inc}(t) + E_{3,inc}(t) \tag{24}$$

2.5.2. Electromagnetic Fields Generated by the Reflected Current Component

In the model, the propagation of the reflected current component is described using the CD type model [9]. In the CD type models, both the injected current and the negative corona currents propagate upwards with the speed of light and the velocity fields associated with these currents are equal to zero. Thus, as in the CG type models, the total electromagnetic fields can again be described as a summation of radiation and static fields. Consider the process taking place in a channel element dz when the return stroke front reaches that current element. The arrival of the return stroke front will generate a corona current which will travel upwards with the speed of light. The radiation field generated by the initiation of the corona current is

$$dE_{1,ref} = \frac{i_{c,r}(z, t - r/c)}{2\pi\varepsilon_0 cr} \frac{\sin^2\theta}{1 + \cos\theta} dz \tag{25}$$

where the corona current is given by Equation (10), but the charge density has to be replaced by $\rho_{ref}(z)$ which was given by Equation (17). That is

$$i_{c,r}(z) = \frac{\rho_{ref}(z)}{\tau(z)} \exp\{-[t - z/v_{av}(z)]/\tau(z)\} \tag{26}$$

The total radiation field generated by the initiation of corona currents along the return stroke channel is given by

$$E_{1,ref}(t) = \int_0^L \frac{i_{c,r}(z, t - r/c)}{2\pi\varepsilon_0 cr} \frac{\sin^2\theta}{1 + \cos\theta} dz \qquad (27)$$

In addition, the upward movement of the reflected current with the speed of light from ground level will give rise to a radiation field given by

$$E_{2,ref} = \frac{I_r(0, t - D/c)}{2\pi\varepsilon_0 cD} \qquad (28)$$

Consider again a channel element at height z. As the negative charge leaves this channel element in the form of corona current, positive charge will remain in the channel element. The positive charge on this channel element as a function of time is given by

$$q_r(z, t)dz = dz \int_{z/v_{av}(z)}^t i_{c,r}(z, t)dt \qquad (29)$$

The static field produced by this charge at the point of observation is

$$dE_{3,ref}(t) = \frac{q_r(z, t - r/c)}{2\pi\varepsilon_0 r^2} \cos\theta dz \qquad (30)$$

The total static field produced by the static charges accumulated along the channel is given by

$$E_{3,ref}(t) = \int_0^L \frac{q_r(z, t - r/c)}{2\pi\varepsilon_0 r^2} \cos\theta dz \qquad (31)$$

Thus, the total electric field produced by the reflected current is given by

$$E_{ref}(t) = E_{1,ref}(t) + E_{2,ref}(t) + E_{3,ref}(t) \qquad (32)$$

Note that the radiation field generated by the reflected current at ground level is opposite to that of the radiation field generated by the absorption of the incident current at ground level. When $f = 0.5$, the two fields cancel each other. This itself is an interesting observation which shows that whenever there is total current reflection, the radiation field generated by the process is equal to zero.

3. Results

The results to be presented in the following subsections are valid for a subsequent return stroke with a 12-kA peak current at ground level.

3.1. Results Pertinent to the Case without Current Reflection

Consider the case where the incident current is absorbed by the ground without current reflection ($f = 1.0$). In this case, the total channel-base current with a 12-kA peak is generated by the incident current component. First, let us illustrate the effect of the ground conductivity at the striking point on the features of the return stroke current.

3.1.1. Effect of the Ground Conductivity on the Return Stroke Current

In their paper, CR showed that the ground conductivity does not influence the peak return stroke current significantly except for very low ground conductivities. The results to be presented here are not very different from the one presented by CR. Any differences

are caused by the different corona discharge time constant profile and the value of the thermalization time used in the calculations.

Here, we present the results corresponding to different ground conductivities at the strike point. In the case of sea water, we adopt values of 5 S/m as the conductivity and 80 as the relative dielectric constant. For soils of conductivities 0.01 S/m, 0.001 S/m, and 0.0001 S/m, we assume that the relative dielectric constant is 10. The channel-base currents for several conductivities at the strike point are shown in Figure 3.
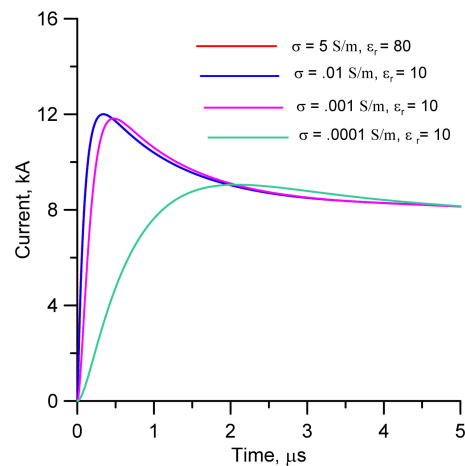
Figure 3. Return stroke current at ground level for four values of the soil conductivity at the strike point. Note that the curves corresponding to $\sigma = 5$ S/m and 0.01 S/m fall on each other.

Recall that the current at ground level is generated by the cumulative effect of corona currents generated along the channel. How fast this charge is collected affects the peak current. As shown in Figure 3, for ground conductivities higher than about 0.001 S/m, the peak current is not much affected by the ground conductivity. The current derivatives for different ground conductivities are shown in Figure 4. Note that the ground conductivity affects the current derivative significantly. The current derivative for 0.0001 S/m is about ten times lower than the current derivative at 0.01 S/m.
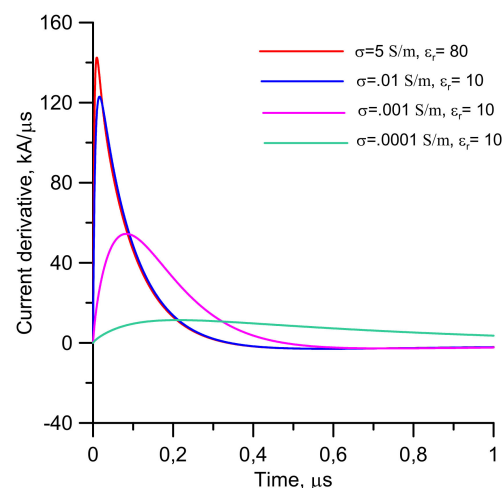

Figure 4. The time derivative of the return stroke current at ground level for four values of the soil conductivity at the strike point.

The reader may wonder whether the general tendency of the effect of the ground conductivity on the peak current is somewhat screened by the assumed rapid increase of the corona discharge time constant with height, i.e., Equation (5). In order to investigate this, we have analyzed the case where the corona discharge time constant remains constant

and equal to its value at ground level along the whole channel. The results obtained for current derivative are shown in Figure 5. Note that the results obtained are not significantly different to the ones shown in Figure 4.
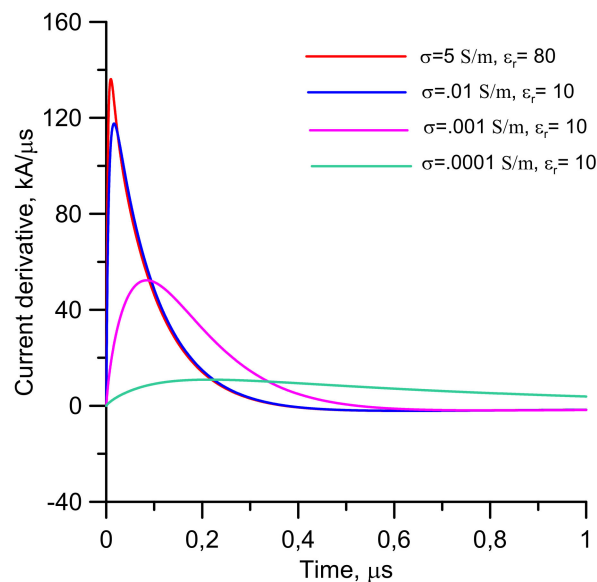

Figure 5. The derivative of the return stroke current at ground level for four values of the soil conductivity at the strike point obtained by assuming that the discharge time constant remains constant along the channel.

The reason why the peak current does not change significantly with the ground conductivity in the high conducting regime (i.e., values greater than about 0.001 S/m) is the following. The peak current is reached when the charge from a channel length approximately equivalent to $t_r v$, where t_r is the risetime of the current and v is the speed of the return stroke at ground level, is collected. If the time taken for this collection process is less than the relaxation time, then the peak current increases as the conductivity is increased. On the other hand, if the time needed for the charge collection process is much longer than the relaxation time, then the peak current would not be much affected by the ground conductivity. In return strokes, the charge collection time is always in the range of hundreds of nanoseconds to microseconds, and, for this reason, the peak current is only affected by very low values of the ground conductivity.

Figure 6 depicts the return stroke current along the channel for two different ground conductivities and permittivities. Figure 6a,b correspond, respectively, to $\sigma = 5$ S/m and $\varepsilon_r = 80$, and to $\sigma = 0.0001$ S/m and $\varepsilon_r = 10$. Observe first that the peak amplitude of the current decreases with increasing height. Second, note that the risetime of the current increases initially and then reaches a more or less constant value. The reason for this feature is our assumption that the corona discharge time constant increases initially but reaches a constant value at higher levels. Observe also that the current risetimes close to the ground in the case of low conductivities are longer compared to those for high conductivities. However, the differences in the risetime become less significant at higher heights along the channel. Of course, this observation is related to some extent to our choice of the corona discharge time constant profile where the discharge time at higher levels is not much modified by the ground conductivity. This is the case because at large heights, the second part of the right-hand side of the Equation (5) becomes larger than the first part. However, had we assumed that the discharge time constant remains the same along the channel, the influence of the ground would have been felt even at higher levels.
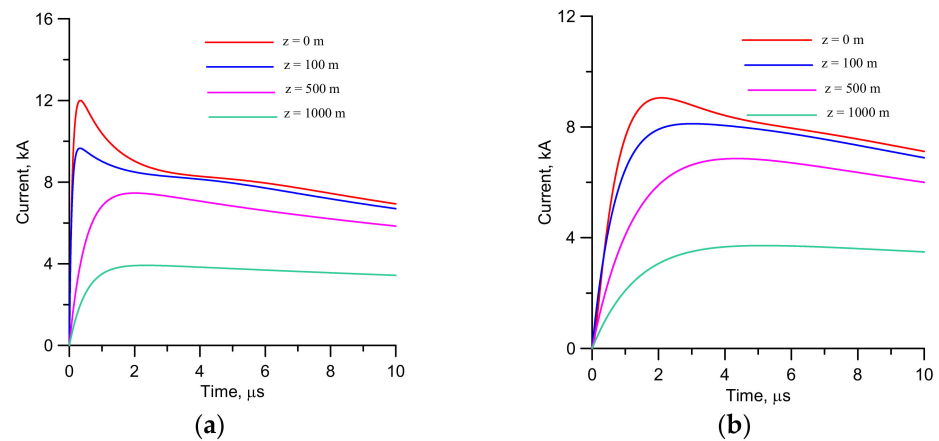
Figure 6. Return stroke current at several heights calculated for (**a**) σ = 5 S/m, ε_r = 80 and (**b**) σ = 0.0001 S/m and ε_r = 10.

3.1.2. Electromagnetic Fields Generated at Different Distances and the Effects of the Ground Conductivity

It is important to point out that the electromagnetic fields given here are the source fields. That is, they are the fields that would be measured if the field propagation to the point of observation is free of propagation effects caused by the finitely conducting ground. In other words, we assume that at the strike point, the ground conductivity is finite, but the path of propagation is along a perfectly conducting ground. One real example where this situation is realized could be the measurement of electromagnetic fields from lightning striking a small island but measured over the surface of the sea. In this case, the source characteristics are affected by the ground conductivity at the strike point, but the resulting fields are not significantly affected by the path of propagation. Another situation where the source fields can be observed without distortion along the propagation path is the measurement of electromagnetic fields at higher altitudes from return strokes. In this case, the source electromagnetic fields appear at the point of observation without being distorted by propagation effects.

Electric Field

The electric field calculated at 50 m, 1 km, and 100 km and the magnetic field at 1 km for several conductivities are shown in Figure 7. The same fields are depicted in an expanded time scale in Figure 8. The close magnetic field resembles the channel base current, and the distant magnetic radiation field has the same temporal features as the electric radiation field. For this reason, the magnetic field is shown only at an intermediate distance. Observe first that the electric fields have all the characteristic features of experimental observations [29,30]. For example, the electric field from subsequent return strokes at 50 m reaches a value close to its peak in a few tens of microseconds. Moreover, the tail of the electric field at around 1 km shows a ramp-like increase and the magnetic field exhibits a pronounced hump. Furthermore, the distant radiation fields cross the zero line at around 40 µs.

Observe that the effect of the conductivity at the strike point does not affect significantly the peak value of the electric field for ground conductivities higher than about 0.001 S/m. However, as in the case of the current peak, for smaller values of the ground conductivity, there is a significant reduction in the peak electric field.
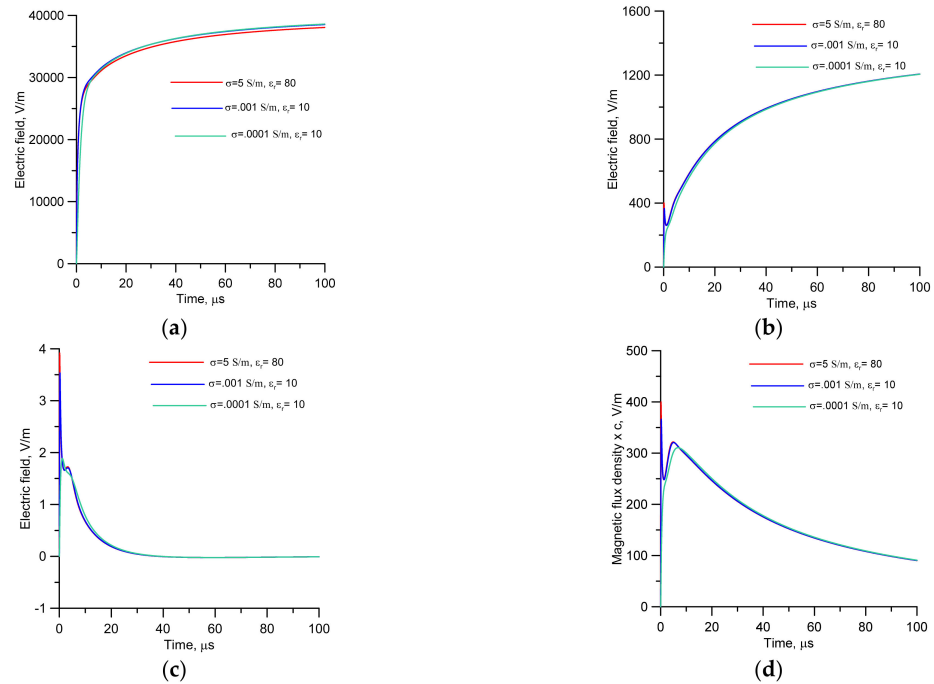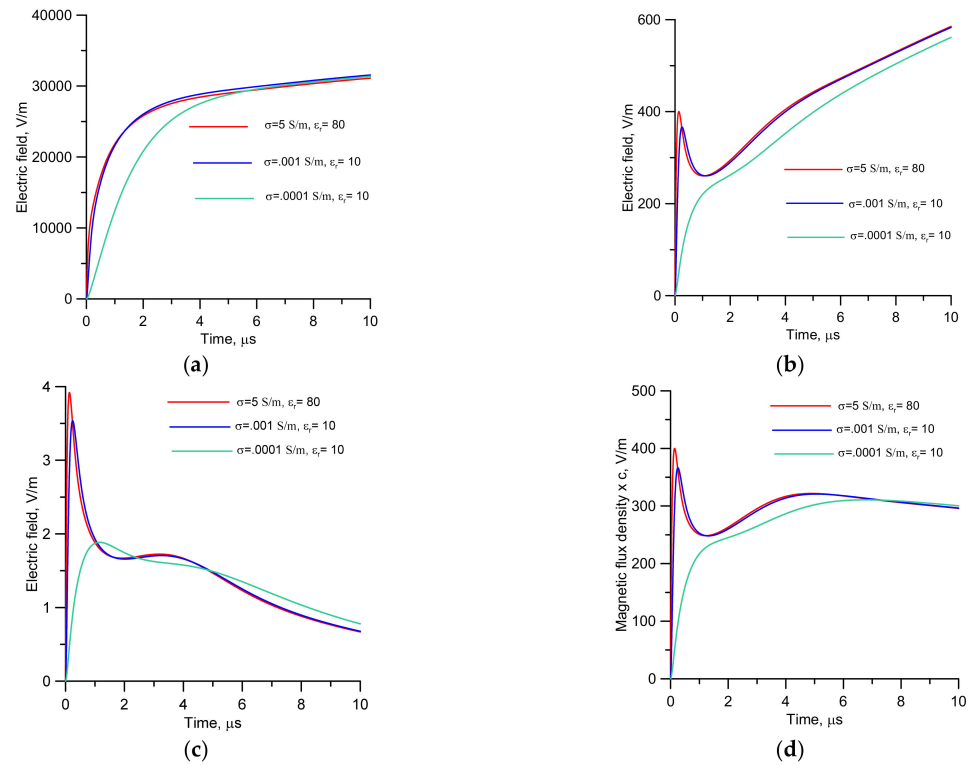
Figure 7. The source electric and magnetic fields generated by a subsequent return stroke of 12 kA for three sets of electric parameters at the strike point. (**a**) Electric field at 50 m, (**b**) electric field at 1 km, (**c**) electric field at 100 km, and (**d**) magnetic field at 1 km (note that the parameter depicted is the product of the magnetic field and the speed of light).

Figure 8. The source electric and magnetic fields generated by a subsequent return stroke of 12 kA for three sets of electric parameters at the strike point. (**a**) Electric field at 50 m, (**b**) electric field at 1 km, (**c**) electric field at 100 km, and (**d**) magnetic field at 1 km (note that the parameter depicted is the product of the magnetic field and the speed of light), but the fields are shown in an expanded time scale.

While defining the profile of the corona discharge time constant, we have mentioned that a discharge time profile that increases monotonically does not generate the subsequent peak in the radiation field. In order to illustrate this, we have reproduced some of the calculations with two other corona discharge time constant profiles. In one case, we have kept the corona discharge time constant uniform along the whole channel and, in the other case, it is assumed to increase linearly with height according to the equation $\tau(z) = \tau_0 + 0.25 \times 10^{-9}z$. The latter variation is identical to that utilized by CR. The resulting radiation field and the magnetic field at 1 km are shown in Figure 9. Note that a corona discharge time constant that remains the same with height or the one that increases monotonically with height does not generate a subsidiary peak in the radiation field. Moreover, such corona discharge time constant profiles will reduce drastically the hump in the magnetic field at intermediate distances.
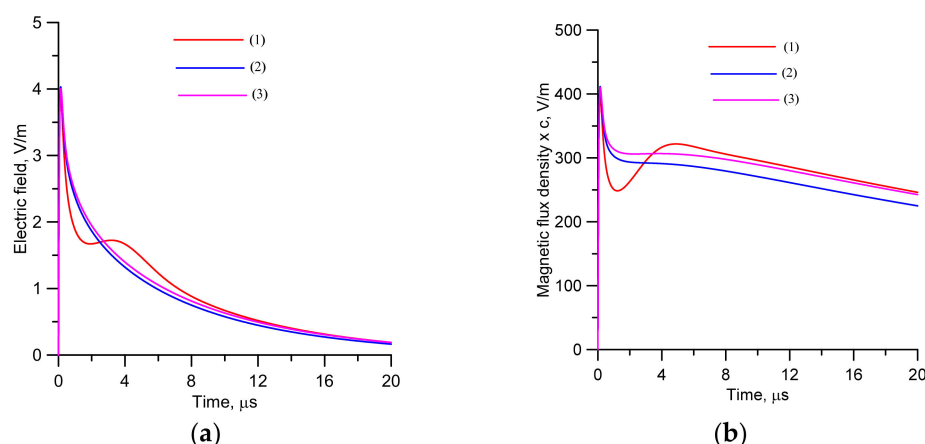

Figure 9. The source electric field (**a**) at 100 km and the source magnetic field (**b**) at 1 km generated by the return stroke for three profiles of the corona discharge time constant. (1) $\tau(z) = \tau_0 + \tau_s(1 - e^{-z^2/\lambda^2})$ (2) $\tau(z) = \tau_0$ (3) $\tau(z) = \tau_0 + 0.25 \times 10^{-9}z$.

Electric Field Derivative

Figure 10 depicts the derivative of the source electric field at 100 km for several soil conductivities at the strike point. Note how, similar to the derivative of the channel-base current, the electric field derivative is significantly reduced by the ground conductivity at the strike point. Observe that the source electric field derivative associated with a strike to sea water is nearly a factor of 3 higher than that for a ground conductivity at the strike point of 0.001 S/m. The ratio is about a factor 20 or more when the ground conductivity is decreased to 0.0001 S/m. Again, we remind the reader that the reduction in the electric field derivative is caused by the influence of the ground conductivity at the strike point on the source characteristics and not due to the propagation effects along a finitely-conducting ground.

It is important to point out that the electric field derivative of the radiation field of a typical subsequent return stroke striking sea water as presented in Figure 10 is somewhat higher than the ones measured over water [31]. However, recall that even the electromagnetic fields propagating over the surface of the ocean are somewhat distorted by propagation effects caused by the finite conductivity and rough ocean surface [32,33]. Thus, we expect the experimentally observed electric field derivatives where the path of propagation is almost over sea water to be less than the values presented above.
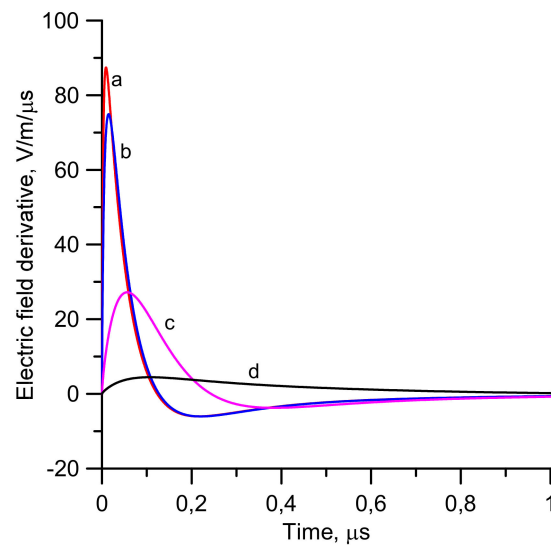
Figure 10. Derivative of the source electric field at 100 km for several electrical parameters of the strike point. (**a**) Sea water: $\sigma = 5$ S/m, $\varepsilon_r = 80$ and (**b**) $\sigma = 0.01$ S/m, $\varepsilon_r = 10$, (**c**) $\sigma = 0.001$ S/m, $\varepsilon_r = 10$, and (**d**) $\sigma = 0.0001$ S/m, $\varepsilon_r = 10$.

It is also important to point out that the peak value of the radiation field derivative of the return stroke striking sea water would be reduced if a larger value for the thermalization time is selected. For example, if the thermalization time is increased from 5 ns to 10 ns, identical to the value used by CR, then the peak derivative of the source radiation field of the return stroke striking sea water will be reduced to about 50 V/m/μs.

3.2. Results Pertinent to the Case with Current Reflection

The results presented earlier concerning the effect of the ground conductivity on the return stroke current do not change when the current reflection at ground level is included in the model. This is the case because the channel base current waveform is still the same at the bottom of the channel. However, the presence of the current reflection would modify the features of the total current at upper sections of the channel and this would affect the features of the electromagnetic field.

Figure 11 shows the electric fields at 50 m, 1 km, and 100 km and the magnetic field at 1 km generated by a subsequent return stroke when the incident current at ground level is completely reflected. Same fields are depicted in an expanded time scale in Figure 12. Results are shown for several conductivities at the strike point. It is important to point out that in this presentation, we are assuming that the amount of current reflected at ground level is independent of the ground conductivity. This may not be the case in reality. Note that in the presence of a current reflection at ground level, the close electric field saturates completely within about 10 μs. This was not the case when there was no current reflection at ground level. In that case, the close field increases rapidly to about 75% of its peak value in a few microseconds, but the rest of the field increases rather slowly to its peak value. The slow rise to the peak value in the case of $f = 1$ is caused by the presence of the field term $E_{2,inc}(t)$. For example, Figure 13 shows the electric field corresponding to $f = 1$ with the three field components depicted separately. It is clear from this diagram that the slow increase in the close field is caused by the term $E_{2,inc}(t)$. However, when $f = 0.5$, the field term $E_{2,inc}(t)$ is cancelled completely by the field term $E_{2,ref}(t)$ and, as a result, the field rises abruptly to its peak value.
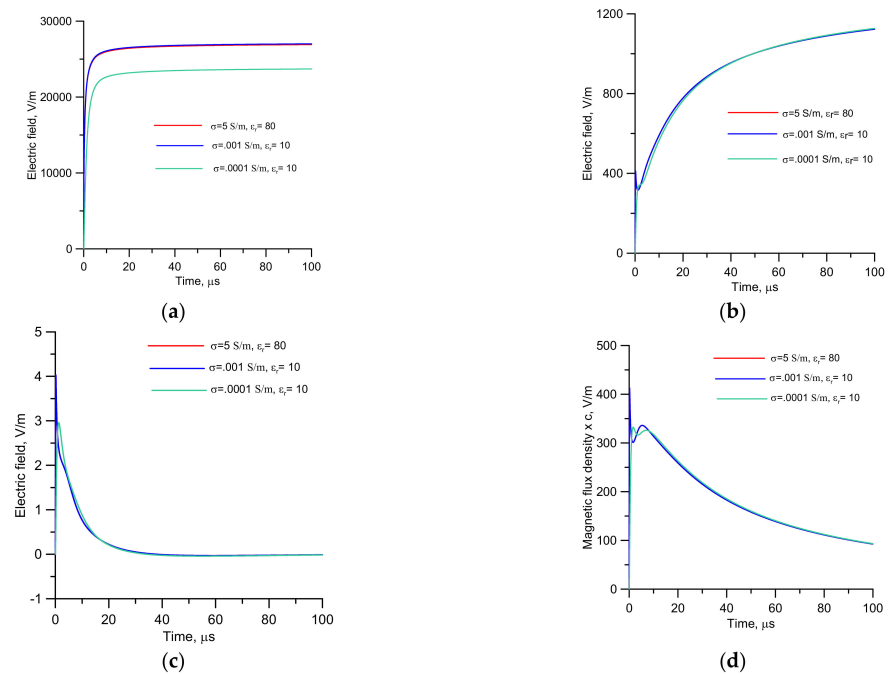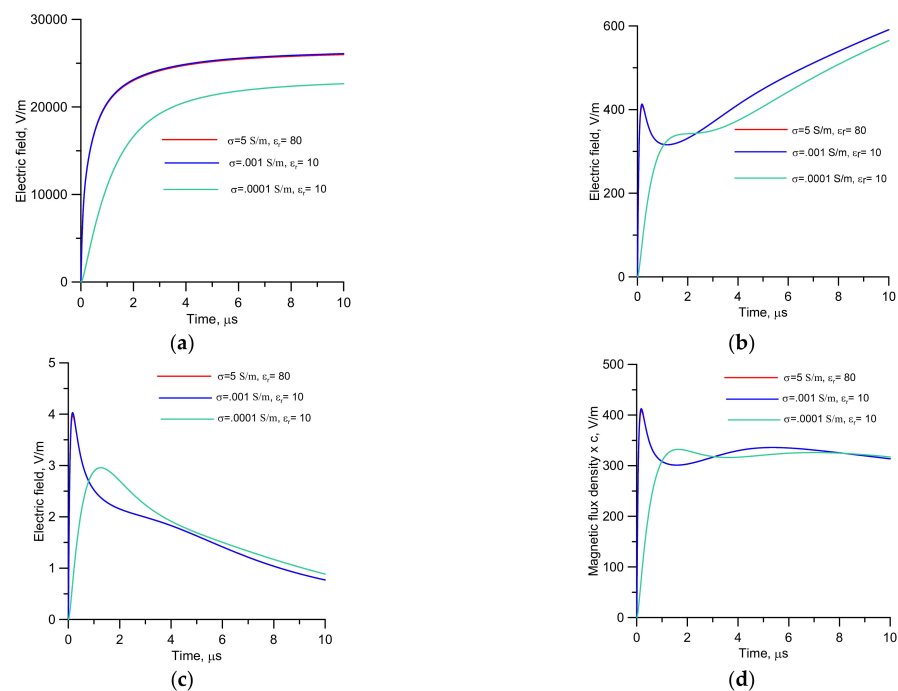
Figure 11. The source electric and magnetic fields generated by a subsequent return stroke for three sets of electric parameters at the strike point when including the current reflection at ground level. (**a**) Electric field at 50 m, (**b**) electric field at 1 km, (**c**) electric field at 100 km, and (**d**) magnetic field at 1 km (note that the parameter depicted is the product of the magnetic field and the speed of light).

Figure 12. The source electric and magnetic fields generated by a subsequent return stroke for three sets of electric parameters at the strike point when including the current reflection at ground level. (**a**) Electric field at 50 m, (**b**) electric field at 1 km, (**c**) electric field at 100 km, and (**d**) magnetic field at 1 km (note that the parameter depicted is the product of the magnetic field and the speed of light), but the fields are shown in an expanded time scale.
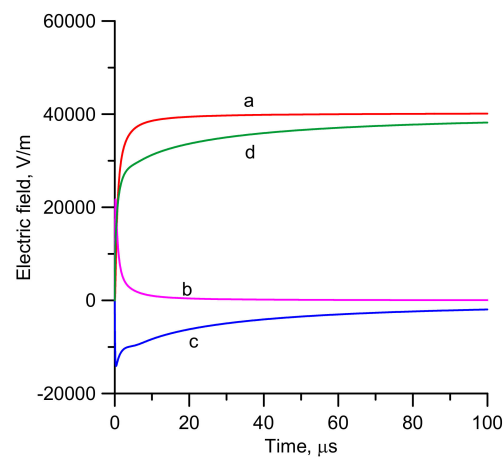
Figure 13. The three components and the total electric field at 50 m corresponding to the case with f = 1.0. (**a**) Static component, (**b**) radiation field generated by the initiation of corona currents, and (**c**) radiation field generated by the absorption of the corona currents at ground level. The total electric field is shown by the curve marked (**d**).

Observe also that the peak value of the close field becomes less when the current reflection is included in the model. The reason for this is the following. Without current reflection, the total current at ground level is generated by the incident component. The charge deposited along the leader channel by this incident current component is given by Equation (4). It is depicted in Figure 14 by the dashed line. Now, when f = 0.5, only half of the current at ground level is the incident current and the charge deposited by this current along the leader channel is half the charge deposited by the incident component in the absence of current reflection. This charge is depicted by curve 'a' in Figure 14. When f = 0.5, the reflected current (half of the total current) is equal to the incident current (half of the total current), and the charge deposited by that current along the leader channel can be calculated from Equation (17). It is depicted by curve 'b' in Figure 14. Now, the total charge deposited along the leader channel is the sum of charges depicted by curves 'a' and 'b' and their sum is depicted by curve 'c'. Comparison of the curve 'c' with the dashed line shows that in the presence of current reflection, the net charge deposited along the section of the leader channel close to ground is smaller than the charge deposited along the leader channel in the absence of current reflection, i.e., the dashed line. Thus, the peak value of the close field decreases in the presence of the current reflection.
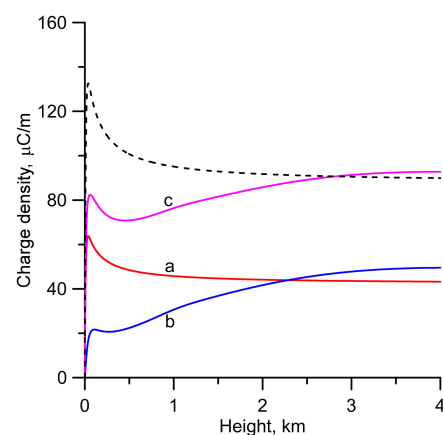

Figure 14. The charge deposited by the incident current (curve a) and by the reflected current (curve b). The total charge deposited by both incident and reflected currents is given by curve c. For comparison purposes, the charge deposited by the incident current in the absence of a current reflection is shown by the dashed line. Note that the total current at ground level with or without the current reflection is equal to 12 kA.

4. Discussion

4.1. Effect of Ground Conductivity on the Current in Laboratory Sparks

The results presented in this paper show that the return stroke current would be not much influenced by the conductivity of the soil at the ground strike point if the conductivity is higher than about 0.001 S/m. However, in a recent paper, Asfur et al. [12] showed that the integrated light intensity of laboratory sparks striking seawater increased with increasing salinity, i.e., with increasing conductivity. Extrapolating this over to return strokes, they claimed that the intensity of the return strokes would be higher with increasing salt concentration in seawater. This claim seems to be in conflict with the results presented in this paper. However, it is doubtful whether the results from laboratory experiments based on small sparks are applicable to return strokes in lightning flashes for the reasons given below.

The reason why the return stroke peak current does not increase with increasing conductivity for conductivities larger than about 0.001 S/m is the fact that the peak current is generated by charges collected over a long channel length. Even though the neutralization of the corona sheath becomes faster with high water conductivity, the peak current is generated by the cumulative effect of all the corona currents resulting from the neutralization process distributed over a length of a few tens to hundreds of meters. Thus, the value of the peak current is decided more by the time it takes for the return stroke to travel a distance of about 100 m or so and not by the rapidity at which the neutralization is achieved. However, in very short sparks, the charge collection time is very short and the peak discharge current is mainly controlled by how fast the neutralization is achieved, i.e., by the relaxation time. Thus, as the relaxation time decreases, the peak current would start to increase. In order to demonstrate this, consider a 10-cm long spark. We assume that the charge distribution along the spark channel is such that it decreases linearly along the channel. The speed of the spark is assumed to be 10^8 m/s. Figure 15 shows the peak current at the strike point for several seawater conductivities. Note how the peak current increases with increasing conductivity. Of course, the results depend to some extent on the thermalization time we have used in the calculation. As discussed in Section 2.2, the thermalization time for small sparks could be in the range of sub nanoseconds. In the calculations presented here, we have assumed that it is equal to 0.1 ns. If the thermalization time was larger, the effect of the conductivity on the peak current would have been less significant.
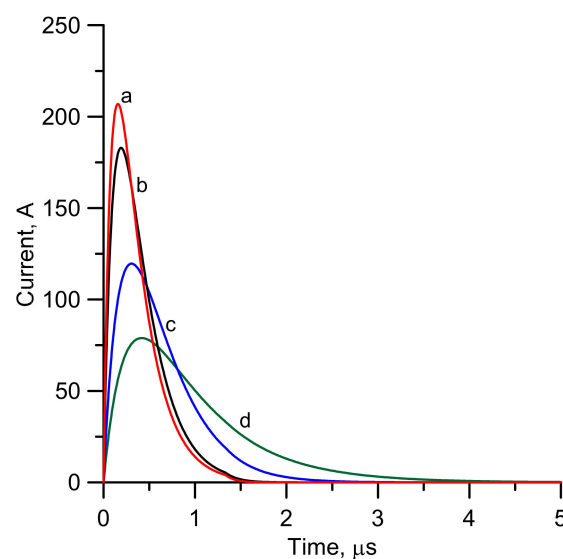

Figure 15. The current at the strike point of a 10-cm long spark for different conductivities of water. (**a**) 10 S/m, (**b**) 5 S/m, (**c**) 2 S/m, and (**d**) 1 S/m.

4.2. Effect of Ground Conductivity at the Strike Point on the Electric Field Derivatives Measured over Finitely Conducting Ground

In a paper published in 1998, Heidler and Hopf [13] analyzed the electric field derivatives measured within a few kilometers from lightning channels striking low conducting soil in Germany. After taking into account the propagation effects along the path of propagation, they still could not explain the low values of the observed electric field derivatives. They concluded that the source electric field derivatives of lightning flashes striking poorly conducting soil in the region where the experiment was conducted were significantly smaller than the electric field derivatives observed under maritime conditions in Florida. Their conclusions agree with our analysis. Our study, presented earlier, shows that the peak electric field derivatives of the source electric fields from lightning flashes striking poorly conducting soils are significantly smaller than the ones generated by lightning flashes striking highly conducting soils. However, if the electromagnetic fields propagate over poorly conducting soil, the electric field derivatives of distant fields could be attenuated to such an extent that it may not be possible to make any conclusions concerning the strength of the source electric field derivatives. In other words, if the attenuation of the fields is very high, it is possible that the distant electric field derivative will exhibit the same strength irrespective of the strength of the source electric field derivative. In order to find out whether the source characteristics could affect the electromagnetic fields measured at a distance over poorly conducting soil, we have conducted the following numerical experiments using the simple propagation model introduced by Cooray and Lundquist [34]. In one set of experiments, we have assumed that lightning strikes salt water, but the propagation path is over a finitely conducting ground. This situation would be similar to the case where the source characteristics are identical to that of maritime conditions and are not affected by the ground conductivity at the striking point. In the second set of numerical calculations, we have considered the case where the lightning flash strikes the finitely conducting soil over which the electromagnetic field propagates. The results obtained for two conductivities and for two propagation distances are shown in Figure 16. In each diagram, the curve labelled i depicts the electric field after propagation assuming that the source fields are identical to those of a return stroke striking sea water and the curve labelled ii depicts the electric field taking into account the effect of the ground conductivity on the source field. Note that in each case the peak of the electric field derivative is significantly larger in (i) than in (ii). Moreover, the half-width of the electric field derivative is smaller in (i) than in (ii). This demonstrates the validity of the conclusion made by Heider and Hopf [13]. That is, lightning return strokes striking highly conducting ground have faster derivatives in source fields than the lightning return strokes striking poorly conducting ground. This, in turn, supports the conclusions made in this paper, namely, that the return stroke currents are affected by the ground conductivity which in turn will affect the electromagnetic fields.

4.3. Extension of the Model to Include Field Changes Due to the Leader

Since the leader charge distribution is one of the input parameters of the model, it could be used in a consistent manner to obtain the combined leader-return stroke electric fields at any given distance from the return stroke. It is important to point out that the leader charge distribution derived by Cooray et al. [14] has been used frequently in estimating the electric field generated by down coming dart leaders and lightning simulation studies [35]. Moreover, as shown by Cooray et al. [14] the resulting fields from the charge distribution are also in agreement with the measured dart leader fields. The charge distribution along the leader channel as it extends towards the ground is given by (after taking into account the risetime of the dart leader):

$$\rho_l(\xi) = k I_p \left(1 - e^{-\xi/\lambda}\right) \left[a_0 \left(1 - \frac{\xi}{H - z_0}\right) \left(1 - \frac{z_0}{H}\right) + \left(1 - \frac{z_0}{H}\right) \frac{(a + b\xi)}{1 + c\xi + d\xi^2} \right] \quad (33)$$
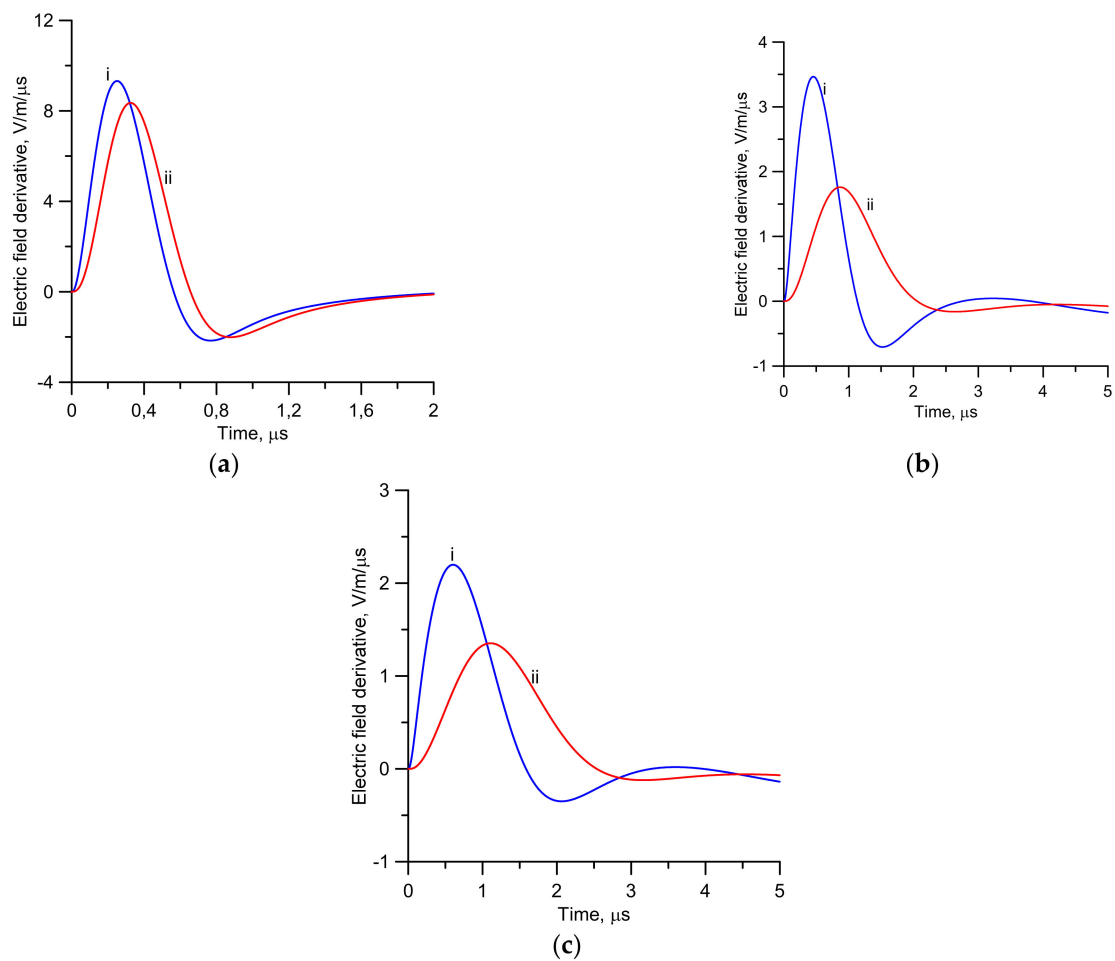
Figure 16. The electric field derivative after propagating (**a**) 2 km over σ = 0.001 S/m, (**b**) 1 km over σ = 0.0001 S/m, and (**c**) 2 km over σ = 0.0001 S/m. Curve (i) corresponds to the results obtained if the source fields are identical to that of striking sea water and curve (ii) corresponds to the results obtained if the source fields are modified by the ground conductivity at the strike point.

In the above equation, z_0 is the vertical height of the tip of the leader, H is the total vertical length of the leader channel in meters, $\rho_l(\xi)$ (in C/m) is the charge per unit length of the leader channel at a point located at a vertical distance ξ from the tip of the leader channel, and I_p is the peak return stroke current in kA. As mentioned earlier, k = 1.4. The above equation is much simpler than the original version published by Cooray et al. [14] but it gives essentially the same leader charge distribution.

Since Equation (33) gives the variation of the leader charge as the leader descends, it can be used to calculate the electric field generated by the leader at any given point. Figure 17 depicts the leader return stroke field at 15, 30, and 50 m for a subsequent return stroke having a 12 kA current at ground level. Note that, in the case of no current reflection, the return stroke completely neutralizes the charge that is stored on the sections of the leader channel close to the ground. This is the case because the return stroke field brings the electric field back to the zero level. However, in the presence of a current reflection, there is a residual field remaining after the return stroke. This is caused by the lower amount of positive charge deposited on the sections of the leader channel close to ground by the reflected current. This point was discussed in Section 3.2. Interestingly, Rakov et al. [30] observed such residual fields in the experimental data obtained from triggered lightning flashes. They attributed these residual electric fields to the presence of charges on the branches which were not neutralized by the return stroke. Similar residual fields were also

observed in Rubinstein et al. [36], but sometimes also with return stroke fields higher than the leader fields.
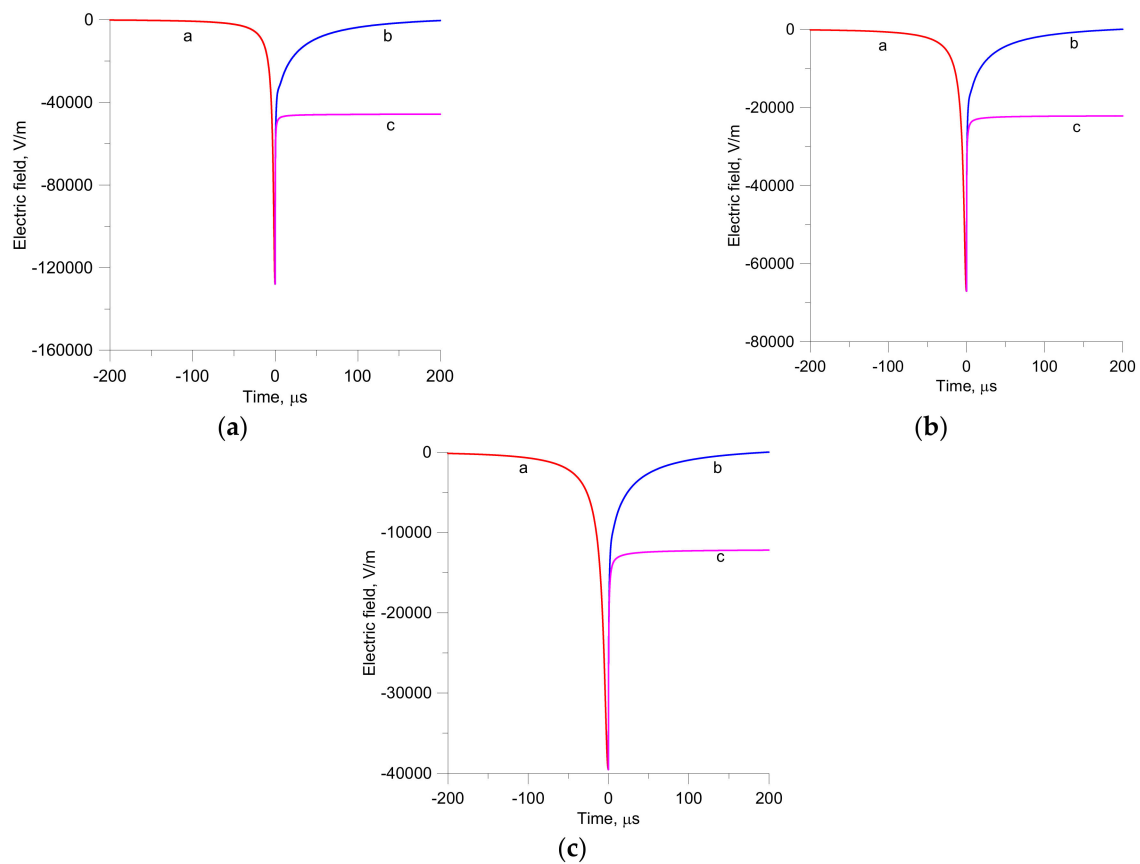
Figure 17. The dart leader-return stroke fields corresponding to (**a**) 15 m, (**b**) 30 m, and (**c**) 50 m from the lightning strike. The curve 'a' corresponds to the leader field. The curve 'b' corresponds to the return stroke field in the absence of current reflection and the curve 'c' corresponds to the return stroke field when the current reflection is included in the model. In the diagrams, the time zero corresponds to the initiation of the return stroke.

5. Further Development of the Model

The model described here is valid for subsequent return strokes. However, our preliminary analysis shows that it could be adapted to represent first return strokes with a slight change of model parameters. First, in the case of first return strokes, the initial phase of the return stroke takes place along the streamer region of the stepped leader where the charge density could be less than that of the fully developed part of the stepped leader channel. Thus, even in the case of first return strokes, one can expect the charge density to increase initially over a length roughly on the order of a step length. The step length in typical stepped leaders close to the ground is on the order of 10 m. This makes λ equal to about 10 m (same as that for subsequent strokes but for different reasons). Second, since the volume of the stepped leader is larger than that of the dart leader, one would expect the thermalization time to be longer than that of the dart leader. Our analysis shows that a thermalization time of about 50 ns is needed to obtain peak electric field derivatives comparable to the measured electric field derivatives at 100 km for lightning flashes striking the sea. Furthermore, the value k is identical to that used for subsequent return strokes (i.e., equal to 1.4). With these parameters, the model can be utilized to study the features of first return strokes.

6. Conclusions

The theory developed by Cooray and Rakov [11] is further extended here to create a return stroke model which is capable of taking into account the possible modifications of the return stroke properties by the soil conductivity at the strike point of the lightning flash. The model is also capable of incorporating the reflection of the current at the ground end of the return stroke channel. Moreover, since one of the input parameters is the charge distribution along the leader channel, the model is capable of generating both dart leader and return stroke fields in a consistent manner. The results show that the peak current and the peak of the source electromagnetic fields are not much affected by the soil conductivity at the strike point for conductivities larger than about 0.001 S/m. However, the peak current and peak fields are reduced by lower conductivities. On the other hand, the application of the same theory, but dimensioned for small sparks, shows that even the variations in the conductivity of sea water (i.e., from 1 S/m to 10 S/m) can influence the peak current, in agreement with the observations of Asfur et al. [12]. The results show that both the current and electric field derivatives are significantly affected by the ground conductivity at the strike point. It is shown that this effect can actually be observed in experiments as demonstrated by the experimental data published some time ago by Heidler and Hopf [13]. The inclusion of the current reflection at ground level significantly influences the saturation of the close electric fields. The current reflection also gives rise to residual electric fields, observed as a difference in the field change generated by the dart leader and the return stroke.

References

1. Cooray, V. Return stroke models with special attention to engineering applications. In *The Lightning Flash*, 2nd ed.; Cooray, V., Ed.; IET Publishers: London, UK, 2014.
2. Uman, M.A.; McLain, D.K. Magnetic field of lightning return stroke. *J. Geophys. Res.* **1969**, *74*, 6899–6910. [CrossRef]
3. Nucci, C.A.; Mazzetti, C.; Rachidi, F.; Ianoz, M. On lightning return stroke models for LEMP calculations. In Proceedings of the 19th International Conference on Lightning Protection, Graz, Austria, 25–29 April 1988.
4. Rakov, V.A.; Dulzon, A.A. A modified transmission line model for lightning return stroke field calculation. In Proceedings of the 9th International Symposium on Electromagnetic Compatibility, Zurich, Switzerland, 12–14 March 1991; pp. 229–235.
5. Cooray, V.; Orville, R.E. The effects of variation of current amplitude, current risetime and return stroke velocity along the return stroke channel on the electromagnetic fields generated by return strokes. *J. Geophys. Res.* **1990**, *95*, 18617–18630. [CrossRef]
6. Cooray, V.; Rubinstein, M.; Rachidi, F. Modified Transmission Line Model with a Current Attenuation Function Derived from the Lightning Radiation Field—MTLD Model. *Atmosphere* **2021**, *12*, 249. [CrossRef]
7. Heidler, F. Travelling current source model for LEMP calculation. In Proceedings of the 6th International Symposium on EMC, Zurich, Switzerland, 5–7 March 1985; pp. 157–162.
8. Diendorfer, G.; Uman, M.A. An improved return stroke model with specified channel base current. *J. Geophys. Res.* **1990**, *95*, 13621–13644. [CrossRef]
9. Cooray, V. A novel procedure to represent lightning strokes–current dissipation return stroke models. *Trans. IEEE* **2009**, *51*, 748–755. [CrossRef]
10. Cooray, V.; Diendorfer, G. Merging of current generation and current dissipation lightning return stroke models. *Electr. Power Syst. Res.* **2017**, *153*, 10–18. [CrossRef]
11. Cooray, V.; Rakov, V. Engineering lightning return stroke models incorporating current reflection from ground and finitely conducting ground effects. *IEEE Trans. Electromagn. Compat.* **2011**, *53*, 773–781. [CrossRef]

12. Asfur, M.; Price, C.; Silverman, J.; Wiskerman, A. Why is lightning more intense over the oceans? *J. Atmos. Sol. -Terr. Phys.* **2020**, *202*, 105259. [CrossRef]

13. Heidler, F.; Hopf, C. Measurement Results of the Electric Fields in Cloud-To-Ground Lightning in Nearby Munich, Germany. *IEEE Trans. Electromagn. Compat.* **1998**, *40*, 436–443. [CrossRef]

14. Cooray, V.; Rakov, V.; Theethayi, N. The lightning striking distance–revisited. *J. Electrost.* **2007**, *65*, 296–306. [CrossRef]

15. Berger, K. Novel observations of lightning discharges: Results of research on Mount San Salvatore. *J. Frankl. Inst.* **1967**, *283*, 478–525. [CrossRef]

16. Kasemir, H.W. A contribution to the electrostatic theory of a lightning discharge. *J. Geophys Res.* **1960**, *65*, 1873–1878. [CrossRef]

17. Cooray, V. *Introduction to Lightning*; Springer: Berlin/Heidelberg, Germany, 2015.

18. Cooray, V.; Idone, V.P.; Orville, R.E. Velocity of a self propagating discharge as a function of current parameters with special attention to return strokes and dart leaders. In Proceedings of the International Conference on Lightning and Static Electricity, Bath, UK, 26–28 September 1989; pp. 14.3.1–14.3.9.

19. Carl, E. *Baum, Electron Thermalization and Mobility in Air, EMP Theoretical Notes, Note XII*; Air Force Weapons Laboratory, Kirtland AFB: Kirtland, NM, USA, 1965.

20. Jordan, D.M.; Uman, M.A. Variation in light intensity with and time from subsequent lightning return strokes. *J. Geophys. Res.* **1983**, *88*, 6555–6562. [CrossRef]

21. Bendjamin, J.; Gomes, C.; Cooray, V. Remote sensing of ESD through optical and magnetic radiation fields. *IEEE Trans. Dielectr. Electr. Insul.* **1999**, *6*, 896–899. [CrossRef]

22. Krehbiel, P.R. The electrical structure of thunderstorms. In *The Earth's Electrical Environment*; Krider, E.P., Roble, R.G., Eds.; National Academy Press: Washington, DC, USA, 1986; pp. 90–113.

23. Cooray, V.; Lundquist, S. Characteristics of the Radiation Fields from Lightning in Sri Lanka in the Tropics. *J. Geophys. Res.* **1985**, *90*, 6099–6109. [CrossRef]

24. Mach, D.M.; Rust, W.D. Photoelectric return stroke velocity and peak current estimates in natural and triggered lightning. *J. Geophys. Res.* **1989**, *94*, 13237–13247. [CrossRef]

25. Schonland, B.F.J. The Lightning Discharge. In *Handbuch Der Physik*; Springer: Heidelberg/Berlin, Germany, 1956; pp. 576–628.

26. Cooray, V. Unification of engineering return stroke models. *Electr. Power Syst. Res.* **2021**, *195*, 107118. [CrossRef]

27. Thottappillil, R.; Uman, M.A. Extension of the Diendorfer-Uman lightning return stroke model to the case of a variable upward return stroke speed and a variable downward discharge current speed. *J. Geophys. Res.* **1991**, *96*, 17143–17150. [CrossRef]

28. Cooray, V.; Cooray, G. The electromagnetic fields of an accelerating charge: Applications in lightning return stroke models. *IEEE Trans.* **2010**, *52*, 944–955. [CrossRef]

29. Lin, Y.T.; Uman, M.A.; Tiller, J.A.; Brantley, R.D.; Beasley, W.H.; Krider, E.P.; Weidman, C.D. Characterization of Lightning Return Stroke Electric and Magnetic Fields from Simultaneous Two-Station Measurements. *J. Geophys. Res.* **1979**, *84*, 6307–6314. [CrossRef]

30. Rakov, V.A.; Kodali, V.; Crawford, D.E.; Schoene, J.; Uman, M.A.; Rambo, K.J.; Schnetzer, G.H. Close electric field signatures of dart leader/return stroke sequences in rocket-triggered lightning showing residual fields. *J. Geophys. Res.* **2005**, *110*, D07205. [CrossRef]

31. Willett, J.; Krider, E.; Leteinturier, C. Submicrosecond field variations during the onset of first return strokes in cloud-to-ground lightning. *J. Geophys. Res.* **1996**, *103*, 9027–9034. [CrossRef]

32. Ye, M.; Cooray, V. Propagation Effects Caused by a Rough Ocean Surface on the Electromagnetic Fields Generated by Lightning Return Strokes. *Radio Sci.* **1994**, *29*, 73–85.

33. Cooray, V.; Ye, M. Propagation Effects on the Lightning-Generated Electromagnetic Fields for Homogeneous and Mixed Sea Land Paths. *J. Geophys. Res.* **1994**, *99*, 10641–10652. [CrossRef]

34. Cooray, V.; Lundquist, S. Effects of propagation on the risetime and the initial peaks of radiation fields from return strokes. *Radio Sci.* **1983**, *18*, 409–415. [CrossRef]

35. Becerra, M.; Cooray, V.; Roman, F. Lightning striking distance of complex structures. *IET Gener. Transm. Distrib.* **2008**, *2*, 131–138. [CrossRef]

36. Rubinstein, M.; Rachidi, F.; Uman, M.A.; Thottappillil, R.; Rakov, V.A.; Nucci, C.A. Characterization of vertical electric fields 500 m and 30 m from triggered lightning. *J. Geophys. Res.* **1995**, *100*, 8863–8872. [CrossRef]